The potential or Green's function for Eq. (4) which is source-like is

$$\phi_s = m/2\pi k \ln [(x - \xi)^2 + k^2(y - \eta)^2]^{1/2} \quad (5)$$

where $k = (1 - F_h^2)^{1/2}$.

A y-directed shallow water dipole is obtained by differentiating with respect to η, taking the form

$$\phi_d = \sigma k/2\pi\{(y - \eta)/[(x - \xi)^2 + k^2(y - \eta)^2]\} \quad (6)$$

Integration over $\xi = \xi'$ from $-\infty$ to ξ gives the potential of a shallow-water vortex located at $x = \xi$, $\eta = 0$ as

$$\phi_v = (\gamma/2\pi)\cdot\tan^{-1}[(x - \xi)/ky^{(\gamma/2\pi)\tan^{-1}(x-\xi/Ry)}] \quad (7)$$

The ship disturbance potential may then be constructed as a distribution of shallow water vortices of unknown strength density $\gamma(x)$ together with the outer flow potential as

$$\Phi = \frac{1}{2\pi}\int_{-l}^{l} \gamma(\xi)\tan^{-1}\left(\frac{x - \xi}{ky}\right) d\xi + V_y y \quad (8)$$

The velocity components induced by this distribution are

$$u(x, y) = \frac{ky}{2\pi}\int_{-l}^{l} \frac{\gamma(\xi)d\xi}{(x - \xi)^2 + (ky)^2} \quad (9)$$

and

$$v(x,y) = -\frac{k}{2\pi}\int_{-l}^{l} \frac{\gamma(\xi)\cdot(x - \xi)d\xi}{(x - \xi)^2 + (ky)^2} + V_y$$

Along the barrier,

$$u(x + 0) = -(\gamma/2)(x) \qquad |x| \leq l \quad (10)$$

$$u(x - 0) = +(\gamma/2)(x)$$

$$v(x,0) = -\frac{k}{2\pi}\int_{-l}^{l} \frac{\gamma(\xi)d\xi}{x - \xi} + V_y \quad (11)$$

Matching Eq. (10) with the inner approximation at large distances from the inner region ($\epsilon \leq y < 1$) gives

$$\gamma(x) = 2(d/dx)(UC) \quad (12)$$

and

$$v(x) = U(x) = \frac{-k}{2\pi}\int_{-l}^{l} \frac{\gamma(\xi)}{x - \xi} d\xi + V_y \quad (13)$$

Combining Eqs. (12) and (13) gives the following equation for the unknown inner stream velocity $U(x)$

$$U(x) = \frac{k}{\pi}\int_{-l}^{l} \frac{(UC)'}{\xi - x} d\xi + V_y \qquad k = (1 - F_h^2)^{1/2} \quad (14)$$

This equation collapses to that developed by Newman when $k = 1$ or $F_h = 0$ as should be obtained. It is also interesting to note that as $C \to 0$ (large water depth) $U \to V_y$ and the gravitational effect also vanishes. As Newman pointed out, it is the familiar integral equation which arises in calculating the lift on a large aspect ratio wing—in his case for zero Mach number, whereas here it corresponds to the Mach number given by $M = F_h$ when we view U as proportional to the lift coefficient, $C_L/2\pi$, C as $\pi c(x)/4$ (c being the chord) and $V_y \approx V_x\alpha$, α being the angle of attack.

It is not at all necessary to solve Eq. (13) in order to find how the forces on a ship vary with Froude number. One need only replace $C(x)$ by $C(x)/k$ to reduce the equation to that for zero Froude number. This means, as in the Prandtl-Glauert rule in subsonic flow, that the flow about a ship at Froude number F_h is equivalent to one whose blockage coefficient is increased by the factor $(1 - F_h^2)^{-1/2}$. This result might have been anticipated at the outset from aerodynamic experience. Of course, the rule is limited to moderate F_h and breaks down as $F_h \to 1$.

This enables the direct use of Newman's results to give the formulas for the added mass, added mass moment of inertia, lateral force and moment about the z-axis in the following forms:

Added mass

$$M_{yy} = -\rho\nabla + \frac{2\rho hLB}{(1 - F_h^2)^{1/2}}\int_1^1 \frac{U_0\bar{C}}{V_y} dx \quad (15)$$

Added mass moment of inertia

$$I_{zz} = \frac{-\rho L^3 S_0}{8}\int_1^1 x^2\bar{S}(x)dx + \frac{\rho hL^3 B}{(1 - F_h^2)^{1/2}}\int_1^1 \frac{U_0\bar{C}}{L\dot{\theta}}(x)xdx \quad (16)$$

Lateral Force

$$Y = +\frac{4\rho hB}{[(1 - F_h^2)]^{1/2}}\left(\frac{\bar{C}(1)U_0(1)}{V_y}\right) U^2\cdot\beta \quad (17)$$

Moment about z-axis

$$N = \frac{LY}{2} + \frac{\rho}{2} LS_0V_x^2\left\{2C_p + \frac{4}{[(1 - F_h^2)]^{1/2}}\left(\frac{hB}{S_0}\right)\int_1^1 \left(\frac{U_0}{V_y}\right)\bar{C}(x)dx\right\}\beta \quad (18)$$

In the above expressions: $\bar{C}$ is the blockage factor divided by ship beam B, S_0 is the maximum cross-sectional area, $\bar{S}$ is the cross-sectional area in fraction of S_0, C_p is the longitudinal prismatic coefficient, and β is the angle of attack $V_y/V_x \ll 1$.

It remains to be seen how well these formulas predict these quantities over a range of Froude numbers and water depths. It is not believed that the terms remaining in the limit $\bar{C} \to 0$ will correctly estimate the infinitely deep results as obtained from model measurements, particularly if the ship model has a skeg at the stern.

References

[1] Newman, J. N., "Lateral Motion of a Slender Body Between Two Parallel Walls," *Journal of Fluid Mechanics*, Vol. 29, 1969, pp. 97–115.

[2] Fujino, M., "Experimental Studies on Ship Maneuverability in Restricted Waters—Part I," *International Shipbuilding Progress*, Vol. 15, No. 168, 1968, pp. 279–301.

[3] Tuck, E. O., "Shallow Water Flows Past Slender Bodies," *Journal of Fluid Mechanics*, Vol. 26, Pt. 1, 1966, pp. 81–95.

Dynamic Similarity Scaling Laws Applied to Cables

M. Lowell Collier Jr.*

Naval Ship Research and Development Center, Calderock, Md.

Nomenclature

A	=	cross-sectional area of cable, L^2
$C_{F,G}$	=	hydrodynamic force (F or G) coefficient/length based on cable diameter, 1
D	=	cable diameter, L
E	=	modulus of elasticity of cable, F/L^2
F	=	hydrodynamic force/length normal to cable, F/L
G	=	hydrodynamic force/length tangent to cable, F/L
M	=	cable mass in air/length of cable, FT^2/L^2
P	=	amplitude of motion, L
R	=	Reynolds number based on cable diameter, 1
T	=	tension in cable, F
U	=	velocity of element of cable normal to static cable configuration, L/T

Received September 20, 1971; revision received November 29, 1971.

* Marine Vessel Vibrations, Program Manager, Towed Systems Branch.

V = velocity of element of cable tangent to static cable configuration, L/T
W = weight/length of cable in water, F/L
a,b,c,d,e,h,i,j,k,l = nondimensional parameters relating model variables to prototype variables, 1
f = frequency, $1/T$
g = gravitational acceleration, L/T^2
ϕ = angle of cable with horizontal, 1
ρ = density of medium surrounding the cable, FT^2/L^4
λ = scaling parameter on length of cable, 1
β = scaling parameter on diameter of cable, 1

Subscript

m = model variable, 1
p = prototype variable
t = time as subscript denotes partial derivative, T
s = cable length as subscript denotes partial derivative, L

Introduction

THERE is an ever increasing need for systems suspended by cables† in the ocean environment. Buoys are moored in the ocean to monitor water quality and weather data. Ship, submarine, or air-towed systems are used for submarine detection, minesweeping, and bottom mapping. Many failures of these systems can be attributed to the dynamic loads in the cable. Although mathematical models are available for predicting the steady-state configuration of a cable system, mathematical models for predicting the dynamic response of cable systems are complex and only limited solutions are possible. Because of the inability to predict dynamic loads on the cable, factors of safety based on the breaking strength of the cable of 4 to 6 are not uncommon.

Scale model testing of cables can give a better understanding of the dynamic behavior of prototype moored or towed systems. Long lengths of cable required for buoy moorings and the difficulty of obtaining data from sea test makes model testing of cables attractive. Model techniques can be applied to a cable if the physical size of the model cable is scaled properly.

Since inertia, viscous and gravity forces are present on the cable two dimensionless numbers that must appear in the nondimensional equations of motion are Froude number and Reynolds number. Oscillating forces caused by buoy or ship motions would be present at one of the boundaries of the cable and thus, Strouhal number must appear. Complete dynamic similarity would be obtained if all dimensionless numbers were satisfied on the model and prototype. In problems where there is one characteristic length it is not possible to obtain complete dynamic similarity. However, since the cable has two characteristic lengths, one of which is much greater than the other (length of cable vs diameter of cable) it is possible to define a distorted scale such that dynamic similarity is obtained. The scaling laws to give this dynamic similarity for a cable are discussed in this paper.

Cable Equations in Normal Coordinates

$$M[(1+\mu)U_t - V\phi_t] + T\phi_s + F(1+\epsilon) + W\cos\phi = 0 \quad (1)$$

$$M[V_t + (1+\mu)U\phi_t] - T_s + G(1+\epsilon) - W\sin\phi = 0 \quad (2)$$

$$(1+\epsilon)\phi_t + U_s - V\phi_s = 0 \quad (3)$$

$$T_t - AE(V_s + U\phi_s) = 0 \quad (4)$$

$$\mu = (M/g)/(M/g + \rho D^2\pi/4) \quad (5)$$

$$\epsilon = T/AE \quad (6)$$

† Cable is used in a general sense to mean wire, rope or chain.

Subscript t and s denote partial differentiation with respect to these variables. These equations assume a cylindrical cross section cable with added mass only due to transverse motion of the cable.

Transformation

In considering a transformation of these equations, the transformation on U and V must be the same and ϕ must transform identically. Therefore,

$$\phi_m = \phi_p, U_m = aU_p, V_m = aV_p \quad (7)$$

where subscripts m and p denote model and prototype, respectively. Let, $M_m = bM_p$, $T_m = cT_p$, $s_m = ds_p$, $(AE)_m = e(AE)_p$, $F_m = hF_p$, $G_m = iG_p$, $t_m = jt_p$, $W_m = kW_p$, $D_m = 1D_p$, where $a, b, c, \ldots 1$ are nondimensional constants. Assuming Eqs. (1–6) apply to the model and substituting Eq. (7) into Eqs. (1–6) gives a new set of equations involving the prototype variables and the constants $a, b, c, d, \ldots$ and 1. This procedure is called the group theory method of obtaining similarity solutions.[1]

From Eq. (5)

$$b = k = 1^2, (W/\rho g D^2), = (W/\rho g D^2)_p \quad (8)$$

From Eq. (6)

$$c = e \text{ or } (T/AE)_m = (T/AE)_p \quad (9)$$

From Eq. (3)

$$aj = d \text{ or } (Ut/s)_m = (Ut/s)_p \quad (10)$$

In Eq. 10, either U or V could be used since both velocities have the same transformation. These components of velocity are the absolute velocity of a cable element and includes any current relative to the cable or flow past the cable due to the cable being towed. Thus, the velocity will not be constant along the length of the cable. A characteristic velocity can be defined and if a nondimensional parameter based on the characteristic velocity is similar on model and prototype this parameter will be similar if based on any other velocity. For a towed cable the characteristic velocity would be the towing speed and for a moored buoy in a current the characteristic velocity would be the current speed. If a buoy is moored in a zero current and subjected to only wave action, the characteristic velocity could be the wave orbital velocity.

From Eqs. (1) and (2)

$$ij/ab = 1, hj/ab = 1, kj/ab = 1, cj/abd = 1$$

or

$$(Ft/UM)_m = (Ft/UM)_p, (Wt/UM)_m = (Wt/UM)_p, (Tt/UMs)_m = (Tt/UMs)_p, (Gt/UM)_m = (Gt/UM)_p \quad (11)$$

From Eqs. (10) and (11), a Froude number based on total length of cable is obtained,

$$(U^2/gs)_m = (U^2/gs)_p \quad (12)$$

Taking

$$s_m/s_p = \lambda \quad (13)$$

$$U_m/U_p = \lambda^{1/2} \quad (14)$$

Using Eqs. (9–14), the other variables become

$$t_m/t_p = \lambda^{1/2} \quad (15)$$

$$E_m/E_p = \lambda \quad (16)$$

Introducing another scaling parameter β such that

$$D_m/D_p = \beta \quad (17)$$

allows the diameter of the cable to be chosen independently of the length scale. The β factor may be greater than, less

than or equal to λ. The other parameters become

$$W_m/W_p = \beta^2 \tag{18}$$

$$M_m/M_p = \beta^2 \tag{19}$$

$$T_m/T_p = \beta^2\lambda \tag{20}$$

Equations (13–20) are all physically realizable transformations. For example, a) U is an input and easily scaled, Eq. (14). b) Time is slower in the model than in the prototype, Eq. (15). Note: The acceleration (velocity per unit time) is the same in model and prototype. c) Soft springs might be used in the model to scale elasticity, Eq. (16). The spring is needed to give the proper influence of elasticity on tension but the spring must not interfere with the transverse cable mot ons. One way to accomplish this is have the cable pass over a sheave before attaching to the spring. The longitudinal wave speed is not scaled properly since there will be reflected waves at the sheave. However, the soft spring being in series with the hard spring (cable), the soft spring will have the greatest influence on the tension. Admittedly elasticity is the most difficult variable to scale properly. d) The weight per foot and virtual mass per foot are proportional to the cable diameter squared for most material, Eqs. (18) and (19) and Table 1. e) The tension is proportional to the total weight of cable and to the total drag force on the cable. The total weight is proportional to diameter squared times length and it will be shown that the total hydrodynamic forces are proportional to diameter squared times length, Eq. (21). Thus, Eq. (20) is physically realizable.

In the case of the hydrodynamic forces F and G, the transformations are not physically realizable. Equation (11) yields

$$F_m/F_p = \beta^2 \tag{21}$$

However

$$F_m/F_p = C_{Fm}/C_{Fp}\rho_m/\rho_p D_m/D_p U_m{}^2/U_p{}^2 \tag{22}$$

where $C_F = C_F(R)$ is the drag coefficient for a cable element perpendicular to the flow and R = Reynolds number based on the characteristic velocity and cable diameter.

$$R_m/R_p = D_m/D_p U_m/U_p \tag{23}$$

neglecting differences in kinematic viscosity. The normal drag F is a function of ϕ but since ϕ transforms identically this functional relation does not appear in Eq. (22).

Other forms of normal drag equations could be used instead of Eq. (22). However, the forms being used for mathematical modeling of cable dynamics are similar to Eq. (22) in that they involve the product of a coefficient that is a function of Reynolds number and a function of cable angle times dynamic pressure.[3]

Substituting the scale factors into Eqs. (22) and (23) and neglecting the difference in ρ_m and ρ_p yields

$$C_{Fm}/C_{Fp} = \beta/\lambda \tag{24}$$

as a requirement on the coefficients and

$$R_m/R_p = \beta\lambda^{1/2} \tag{25}$$

Table 1 Mooring lines weight per unit length approximately proportional to size squared

Nylon			Chain (stud link)			Wire rope (6 × 19)		
D	wt/100 ft	W/D^2	D^b	wt/15 fathoms	W/D^2	D	wt/100 ft	W/D^2
0.25	1.5	24.0	...	...	...	$\frac{1}{4}$	10	160
0.5	6.1	24.4	1	900	900	$\frac{1}{2}$	40	160
0.96[a]	24.5	26.6	2	3,525	883	1	160	160
1.91[a]	100	27.4	3	8,035	894	2	640	160
3.82[a]	416	28.4	4	14,000	882	2.75	1210	160

[a] Circumference/π; [b] size designation.

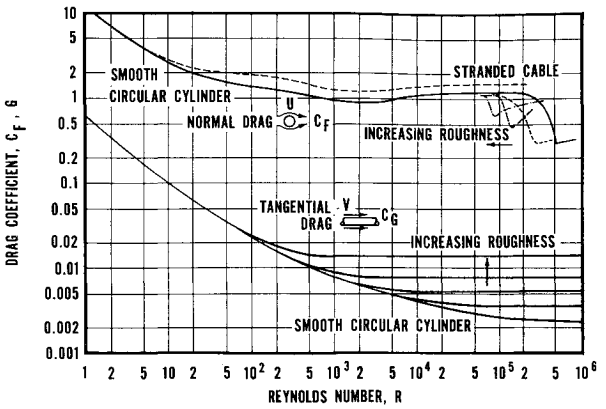

Fig. 1 Normal and tangential drag coefficient vs Reynolds number on smooth and rough circular cylinders.

as a concurrent condition on the Reynolds number. Equations (24) and (25) are additional similarity relations that must be satisfied. Thus, the scale factor λ is chosen on the basis of the length of cable and β is determined from Eqs. (24) and (25) such that C_{Fm} and R_m are points on the drag vs Reynolds number curve for the model cable chosen. Figure 1 is one example of a drag curve. It should be noted that if $\beta = \lambda$ the Reynolds number of the model would be less than the prototype Reynolds number but the drag coefficient would be the same on the model and prototype. This is true only over a limited range of Reynolds numbers. The damping of the cable vibrations depends on modeling the drag function and if $\beta = \lambda$ the drag forces are not dynamically similar. Thus, by using a distorted scaling (length scale different than diameter scale) the damping forces on the cable are dynamically similar.

It is expected that this distorted scaling would be a good model if the cable oscillatory velocity is everywhere small compared to the characteristic velocity (current or towing speed). For a vibrating cable at zero speed other drag functions may be needed. The method would still apply if these new functions were Reynolds number dependent.

Example

The curve shown in Fig. 1 is the normal and tangential drag coefficient vs Reynolds number for smooth and rough circular cylinders.[2] Assume the prototype Reynolds number is about 10^5. From Fig. 1 $C_{Fp} = 1.2$. This is approximately the Reynolds number for a 2-in. diam cable in a flowfield equivalent to a buoy heaving in a sea state 5 or 6. Four values of λ are shown in Table 2 and the equations to be satisfied are $C_{Fm} = 1.2\beta/\lambda$, $R_m = 10^5\beta\lambda^{1/2}$, for each value of λ.

A trial and error solution for β is obtained such the C_{Fm} and R_m are values on the curve of Fig. 1. Table 2 lists the solution for β for several values of λ.

In this case β is significantly different from λ only for very small λ because C_F is nearly constant over the range of R from 10^2 to 10^5. If the R of the prototype was of the order of 10^3 then the difference between λ and β would have been observed for larger λ.

Since β has been chosen to achieve similarity based on the normal drag, the tangential drag coefficient is determined.

Table 2 Scale ratios for dynamic similarity

λ	β	R_m	C_{Fm}
0.05	0.042	939	1
0.02	0.022	310	1.3
0.01	0.0125	125	1.5
0.001	0.0025	7.9	3

This tangential drag coefficient on the prototype will depend on cable roughness whereas the model Reynolds number may be low enough that the coefficient is independent of roughness. Thus, similarity on tangential drag will depend on prototype roughness and may not be satisfied. For forced oscillations of bare cables the largest displacements will be normal to the cable and lack of similarity in the tangential force will not change significantly the cable tension or amplitude of motion.

In Eq. (19) the velocity U is shown to scale as $\lambda^{1/2}$. In the case of a buoy heaving and surging in a seaway or a heaving or pitching ship towing a depressor the velocity is proportional to an amplitude times a frequency, $U = Pf$. Since frequency is angle per unit time, f scale as $\lambda^{-1/2}$. Thus, the amplitude of the input P scales as λ.

$$P_m/P_p = \lambda, f_m/f_p = \lambda^{-1/2} \tag{26}$$

A Strouhal number based on the amplitude of the cable motion at a boundary is thus satisfied on model and prototype. These equations complete the scaling laws required to test models of cable.

References

[1] Hansen, A. G., *Similarity Analyses of Boundary Value Problems in Engineering*, Prentice-Hall, Englewood Cliffs, N.J., 1964.

[2] Wilson, B. W., "Characteristics of Anchor Cables in Uniform Ocean Currents," TR 204-1, 1960, Texas A and M Research Foundation, College Station, Texas.

[3] Casarella, M. J. and Parsons, M., "Cable Systems Under Hydrodynamic Loading," *Marine Technology Society Journal*, Vol. 4, No. 4, July–Aug. 1970, pp. 27–44.

Holographic Interferometry of a Submarine Wake in Stratified Flow

ARVEL B. WITTE*
TRW Systems Group, Redondo Beach, Calif.

A NEW technique, holographic interferometry, has been used to visualize a submarine wake in stratified flow. Shadow and schlieren techniques have been used by other investigators to study stratified flows, but examples of interferometry have not been reported. Pao[1] used the shadow technique to study qualitatively the structure of turbulence in the wake of a cylinder towed through a stably stratified salt water solution. Mowbray[2] used the schlieren technique to study internal waves in a density stratified fluid. The inherent advantages of using interferometry rather than schlieren or shadow techniques to extract quantitative data about flows, have been discussed elsewhere.[3] The specific advantages afforded by using holography, for example, 1) the use of nonprecision optics, 2) depth focusing, and 3) three-dimensional viewing of the flowfield, may make this technique valuable in recording and reducing three-dimensional holographic interferograms to three-dimensional density field. The purpose of this note is to describe the experimental technique and show and discuss some of the experimental results.

A self-propelled model submarine, about 1 in. in diameter and $4\frac{1}{2}$ in. long, was operated in a plexiglas tank 4 ft long and 1 ft square. The submarine was guided by a pair of 0.010-in. wires and powered by a d.c. power supply. A hologram of the submarine in pure water is shown in Fig. 1. A 1-in.-mesh grid, slightly tilted with respect to the plane of the picture, is shown along with the guide wires and power leads. In the experiments which followed the submarine was positioned 2 in. below the water surface and 6 in. above the bottom of the tank. The top 2 in. were pure water; the bottom 6 in. were salt water (NaCl) having a salt mass fraction of 0.01.

The pulsed ruby laser holograph used to record the holographic interferogram has been used in the study of high-speed projectile wakes and is described elsewhere.[4] Because the holographic process records both amplitude and phase a common path interferometer is used in which double exposure of the comparison scene hologram and the test scene hologram is made sequentially in time on one photographic plate. The superposition of these two holograms forms the interferogram. Modification to the holocamera to record the stratified flow pictures was minor. An additional tank of water having the same optical path length as the one in the test section containing the submarine, was placed in the reference beam of the laser to maintain longitudinal coherence of the holocamera.

A finite fringe holographic interferogram of the submarine wake recorded at 4 body lengths behind the submarine moving at 4 fps is shown in Fig. 2. The vertical wires shown in the lower third of the picture are evenly spaced across the width of the tank and serve as objects to focus on when utilizing the depth focusing property of holography. Changes in index of refraction were caused by fluid displacements attending the submarine passage and turbulent wake mixing processes. The nominally vertical parallel fringes observed in the lower portion of the picture denote the undisturbed background fringe pattern. The shifted, irregularly shaped fringes observed in the upper two-thirds of the picture are caused by the changes in the aforementioned refractive index. The fringe shift from the undisturbed position measures the integrated change in refractive index along the light path. Shifts to the left or right denote an increase or decrease in average optical path, respectively.

Two observations which are immediately apparent are that 1) the wake forms an irregular fringe pattern of fringe shift equal to about 1 to 3 fringes (this pattern runs across the central part of the picture), and 2) water cooling at the air-water interface caused a large fringe shift denoting an increase in optical path there.

The fringe shift in the wake is order one. Had a cylinder of uniformly mixed pure and salt water resulted from the passage of the submarine, the fringe shift would have been about 25 fringes. Thus, at 18 submarine diameters it appears

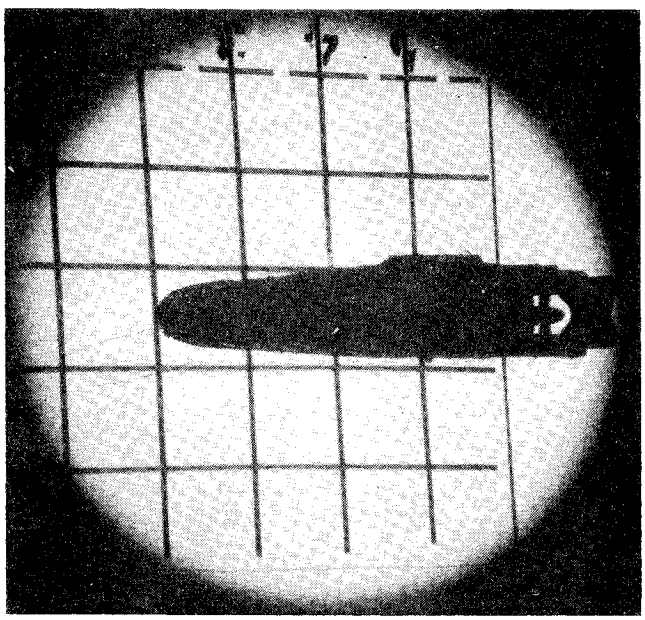

Fig. 1 Hologram of submarine in pure water.

Received October 4, 1971.

* Head Experimental Staff, Fluid Mechanics Laboratory.